Simple Photoreduction of Graphene Oxide Nanosheet under Mild Conditions

Yasumichi Matsumoto,*,†,‡ Michio Koinuma,*,†,‡ Su Yeon Kim,§ Yusuke Watanabe,† Takaaki Taniguchi,†,‡ Kazuto Hatakeyama,† Hikaru Tateishi,† and Shintaro Ida||

Graduate School of Science and Technology, Kumamoto University, 2-39-1 Kurokami, Kumamoto, 860-8555, Japan, JST, CREST, 5 Sanbancho, Chiyoda-ku, Tokyo, 102-0075, Japan, Center for Intelligent Nano-Bio Materials (CINBM), Department of Chemistry and Nano Science, College of Natural Science, Ewha Womans University, Seoul, 120-750, Korea, and Department of Applied Chemistry, Faculty of Engineering, Kyushu University, 744 Motooka, Nishi-ku, Fukuoka, 819-0395, Japan

ABSTRACT Graphene oxide (GO) nanosheets were reduced by UV irradiation in H_2 or N_2 under mild conditions (at room temperature) without a photocatalyst. Photoreduction proceeded even in an aqueous suspension of nanosheets. The GO nanosheets reduced by this method were analyzed by X-ray photoelectron spectroscopy and Raman spectroscopy. It was found that epoxy groups attached to the interiors of aromatic domains of the GO nanosheet were destroyed during UV irradiation to form relatively large sp^2 islands resulting in a high conductivity. $I-V$ curves were measured by conductive atomic force microscopy (AFM; perpendicular to a single nanosheet) and a two-electrode system (parallel to the nanosheet). They revealed that photoreduced GO nanosheets have high conductivities, whereas nonreduced GO nanosheets are nearly insulating. Ag^+ adsorbed on GO nanosheets promoted the photoreduction. This photoreduction method was very useful for photopatterning a conducting section of micrometer size on insulating GO. The developed photoreduction process based on a photoreaction will extend the applications of GO to many fields because it can be performed in mild conditions without a photocatalyst.

KEYWORDS: graphene oxide • nanosheet • thin film • photoreduction • photopatterning • conductive atomic force microscopy

INTRODUCTION

Graphene nanosheets are a promising material for applications in many fields because they have many excellent physical properties (1−6), although they have been reported to be toxic recently (7−10). Graphene nanosheets can be synthesized by various processes (1−15). Synthesis of graphene or reduced graphene oxide (GO) nanosheets from graphite oxide is a very simple method that is inexpensive and capable of large-scale production (16). GO nanosheets can be used as nanoparts for fabricating hybrid nanomaterials that combine with functional molecules by electrostatic principle (16, 17) and/or that have reactive oxygenated functions on their surfaces (16). Low-conductivity GO nanosheets must be reduced to graphene or reduced GO nanosheets that have high conductivities before they can be used in practical devices that require high-conductivity components. In this process, GO nanosheets are initially synthesized by exfoliation of graphite oxide.

The GO nanosheet is then generally reduced by hydrazine, heat treatment in a reducing environment (18−30), or by light irradiation using an intense light source such as laser (31−33) or photocatalyst such as TiO_2 or ZnO (7, 34−38). However, these reduction processes have some disadvantages for the fabrication of some devices, especially using organic and/or biomaterials together with GO. Chemical and photocatalytic methods for reduction introduce heteroatomic and/or adsorbed impurities to the GO nanosheet surface. In the case of the hydrazine method, some hard reduction conditions will sometimes give some damages to the above materials in the device as well as N doping into GO nanosheet during the process (22, 24, 27). The photocatalysts reduce GO nanosheet by the photoproduced electron in the conduction band during the irradiation (7, 34−38). However, the photocatalysts may simultaneously give some damages to the organic or biomaterials in the devices because of strong oxidizing ability of the photoproduced hole during the irradiation. On the other hand, the high temperatures generated by heat treatment are sometimes detrimental to device fabrication. Intense light irradiation methods will also have the same disadvantage as the heat-treatment method, since it is based on the photothermal effect, that is, the heat-treatment effect in principle. Thus, the development of a simpler reduction process that employs mild conditions is desirable for extending the applications of GO.

This paper presents a simple reduction process of GO under mild conditions (room temperature) using relatively weak light irradiation in H_2 or N_2 without a photocatalyst. This process is based on a photoreaction of the GO nanosheet in the mechanism. In addition, photopatterning based on this photoreduction process and the catalytic effect of Ag^+

* Corresponding author. E-mail: yasumi@gpo.kumamoto-u.ac.jp (Y.M.); koinuma@chem.kumamoto-u.ac.jp (M.K.).
Received for review June 17, 2010 and accepted November 9, 2010
† Kumamoto University.
‡ CREST.
§ Ewha Womans University.
|| Kyushu University.
DOI: 10.1021/am100900q

are demonstrated. A hopping and/or tunneling mechanism is proposed for conduction in reduced GO in which electrons move via sp^2 islands produced by reduction in the sp^3 regions of some epoxy and hydroxyl groups at the reduced GO surface (39, 40). In this paper, the conductivities of the GO reduced by the present method are also measured and discussed. The present reduction process was found to increase the GO conductivity by 10^5−10^7 times.

EXPERIMENTAL SECTION

Pure graphite (New Metals and Chemicals Ltd., 99.9999%) powder (0.5 g) was oxidized by Hummers' method (41) in which $NaNO_3$ (0.5 g), H_2SO_4 (23 mL), and $KMnO_4$ (3 g) were mixed in an ice bath and H_2O_2 solution (30%, 3 mL) and H_2O (40 mL, distilled water) were then added at a high temperature (35−95 °C). The resulting mixture was washed several times with distilled water and then dried in an oven. The resulting GO was suspended in distilled water (1.2 mg/mL), sonicated in an ultrasonic bath for 2 h, and centrifuged to remove any aggregated GO. Exfoliated GO was collected in a vial (nanosheet suspension). Unless otherwise stated, the following five samples were irradiated for 2 h with light from a 500 W high-pressure Hg lamp where 99.99% H_2 or N_2 at 1 atm was flowed through a quartz cell containing the GO sample at a rate of about 50 mL/min. The light intensity was about 67 mW/cm^2, and the light source was positioned at a distance of about 40 cm from the sample surface. Samples 1 and 2 were aggregated GO nanosheet films that had been prepared by dropping the nanosheet suspension onto Pt metal and ITO glass substrates, respectively, and then drying them in a vacuum. Sample 1 was used for X-ray photoelectron spectroscopy (XPS) analysis because the Pt substrate has a high conductivity and contains very little oxygen on its surface, making it the most suitable substrate for this measurement. XPS (Sigma Probe, Thermo Scientific, US) was performed in a vacuum better than 10^{-7} Pa. The spectrometer is equipped with a monochromatized X-ray source (Al Kα, $h\nu$ = 1486.6 eV). Electrons emitted from the samples were detected by a hemispherical energy analyzer equipped with six channeltrons. The overall energy resolution for XPS was below 0.55 eV (on Ag $3d_{3/2}$ with a pass energy of 15 eV). The XPS peaks were deconvoluted using Gaussian components after Shirley background subtraction. Raman spectroscopy was performed using a micro Raman spectrometer (NRS-3100, Jasco, Japan) with a 532 nm excitation source at room temperature. Scanning electron microscopy (SEM) measurements were performed using a field-emission scanning electron microscope (Hitachi, SU-8000, Japan) at 5 kV in secondary electron imaging mode. Sample 2 was used for the photopatterning procedure because of the good adhesion between GO and the ITO substrate.

Sample 3 was a GO nanosheet film prepared by dipping a mica substrate into the nanosheet suspension. It was used for atomic force microscopy (AFM; Nanoscope V, Digital Instruments, US) measurements because it has a smooth atomic level surface and good adhesion between the film and the substrate. Almost all the nanosheets of samples prepared by dipping were single. Sample 4 was a GO nanosheet film prepared by dipping highly oriented pyrolytic graphite (HOPG; ZYB quality, NT-MDT) into the nanosheet suspension. It was used for conductivity measurements by conductive atomic force microscopy (C-AFM; Digital Instruments, Nanoscope V, US) using a Pt−Ir AFM tip. The I−V curves measured by this technique represent the conductivity perpendicular to a single nanosheet. HOPG is the most suitable substrate because the surface has a smooth atomic level surface and a high conductivity. HOPG was cleaved using scotch tape immediately prior to immersion. A two-electrode system was used to measure the conductivities parallel to single and aggregated nanosheet films. Single GO and aggregated nanosheet films were prepared by dipping and dropping methods, respectively, using a glass substrate with two comb Au electrodes which were 90 nm thick and were separated by 2 μm. The electrode comb consisted of 60 pairs in the electrode bars (Supporting Information, Figure S1). Sample 5 was the nanosheet suspension. The suspension was directly irradiated, and their UV−vis spectra (V-550, Jasco, Japan) were obtained before and after the photoreduction in H_2. For hydrazine reduction, a GO suspended solution (10 mL) was loaded in a round-bottom flask, hydrazine hydrate (19.3 mmol) was added, and the solution was heated in an oil bath at 100 °C under a water-cooled condenser for 24 h. Over this time, the reduced GO gradually precipitated out as a black solid (24).

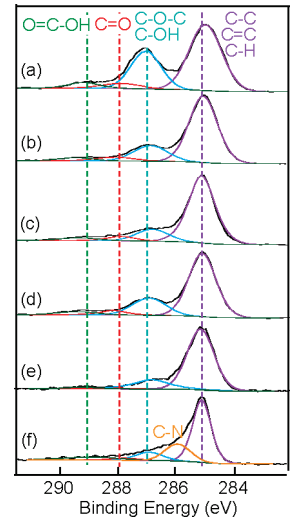

FIGURE 1. XPS spectra of C (1s) for aggregated nanosheet samples (sample 1): GO nanosheet (a) before photoreduction, (b) after photoreduction in H_2 for 2 h, (c) after photoreduction in H_2 for 5 h, and (d) after photoreduction in N_2 for 2 h. (e) Ag^+ adsorbed sample after photoreduction in H_2 for 2 h and (f) reduction by hydrazine. The substrate temperature was lower than 40 °C during photoreduction.

RESULTS AND DISCUSSION

Figure 1 shows C (1s) XPS spectra of sample 1. The deconvoluted peak at a binding energy of 285 eV is attributed to C−C, C═C, and C−H bonds. The deconvoluted peaks centered in the binding energy ranges of 286.8−287.0, 287.8−288.0, and 289.0−289.3 eV are, respectively, attributed to the C−O (C−O−C and C−OH), C═O, and O═C−OH oxygen-containing carbonaceous bands (24, 27, 42−44). The peak intensities of the binding energies of oxygenated groups such as epoxy C−O−C (which probably contains hydroxyl C−OH) decreased with the present photoreduction (Figure 1b−e), and the reduction degree increased with increasing irradiation time (Figure 1b,c). Similar photoreduction occurred even in N_2 (Figure 1d). These results suggest that mainly the C−O−C epoxy bond is decomposed (probably with release of O_2) to produce sp^2 domains (islands) during light irradiation, because the C−O−C peak intensity is mainly reduced by photoreduction. The result for GO treated by hydrazine is also shown to compare it with the present photoreduction treatment, where mainly C−O−C is reduced on the basis of the reduction in the C−O−C peak intensity (Figure 1f). There is an additional component at 285.9 eV, which corresponds to carbon in the C−N bonds (22, 24). Thus, hydrazine treat-

Table 1. Peak Area (A) Ratios of Oxygen-Containing Bonds to CC Bonds (Obtained by XPS) and Peak Intensity Ratios of I_D/I_G (Obtained by Raman Analysis)

	XPS				Raman
	A_{C-O}/A_{CC}	$A_{C=O}/A_{CC}$	A_{OCOH}/A_{CC}	O/C	I_D/I_G
graphene oxide	0.52	0.09	0.08	0.44	1.12
photoreduction in H_2 for 2 h	0.27	0.08	0.06	0.24	1.02
photoreduction in H_2 for 5 h	0.20	0.06	0.06	0.22	0.96
photoreduction in N_2 for 2 h	0.32	0.08	0.07	0.29	1.03
Ag^+ adsorption and photoreduction in H_2 for 2 h	0.26	0.01	0.02	0.18	0.98
reduction by hydrazine	0.20	0.06	0.15	0.24	1.20

ment is very effective for the reduction. The XPS spectrum of the sample adsorbed with Ag^+ was measured after photoreduction; Ag^+ was adsorbed on GO nanosheets by immersing sample 1 in 0.04 M $AgNO_3$ solution and then washing it with water. Figure 1e shows the XPS spectrum of the Ag^+ adsorbed sample. Photoreduction of the GO nanosheet is promoted by the adsorbed Ag^+ (by comparing the two spectra of the 2 h irradiated samples shown in Figure 1b,e). Photoreduction occurred even when a UV cutoff filter (<420 nm) was used to generate visible light irradiation, although the degree of reduction was low. On the other hand, UV irradiation using a visible-light cutoff filter (>390 nm) caused photoreduction with the same degree of reduction as when no filter was used. This demonstrates that UV irradiation is very effective in reducing GO nanosheets. Table 1 lists the peak area ratios of the oxygenated groups and the atomic ratios of O/C of all the samples. Although the degree in the reduction of GO using the present method was lower than those using the heat treatment method (30), it was almost the same as the cases using the photocatalytic reduction method (7, 35).

Epoxy groups are present on the basal planes of GO, and they are relatively unstable (16, 45). In the reduction process, $\pi-\pi^*$ excitation of electrons in sp^2 domains on the GO surface initially occurs during UV irradiation. The generated electron−hole pairs then move to the epoxy groups and break C−O−C bonds, releasing O_2 and forming relatively large sp^2 domains. Ag^+ may promote the destruction of the C−O bond and/or O_2 release in the present photoreduction. Shen et al. (46) have reported that the reduction of GO proceeds with formation of Ag nanoparticles from Ag^+ under the presence of ethylene glycol and $NaBH_4$. They have suggested that the strong interaction may exist between the Ag nanoparticles and the remaining surface hydroxyl O atoms.

The usual characteristics of Raman spectra of carbon materials are the G band (~1580 cm^{-1}), which is generally attributed to the E_{2g} phonon of sp^2 atoms, and the D band (~1350 cm^{-1}), which is a breathing mode of κ-point phonons with A_{1g} symmetry (47, 48) and is attributed to local defects and disorder (49). All the spectra contain the G and D bands. The Raman spectra shown in Figure 2 contain the G band at about 1603 cm^{-1} and the D band at about 1347 cm^{-1}. The ratio of the intensities of the D and G bands (I_D/I_G) are also presented in Table 1. I_D/I_G decreases from 1.12 to 1.02 and 1.03 after 2 h of photoreduction in H_2 and N_2, respectively. Since I_D/I_G is inversely proportional to the in-plane sp^2 domain size (50, 51), this result indicates the formation of relatively large sp^2 domains after photoreduction of the GO, which agrees well with the XPS results. Similar results have been reported for thermal and photocatalytic reduction processes (38, 52). A greater reduction in I_D/I_G was observed when Ag^+ was adsorbed on the sample (0.98), which implies that Ag^+ has a catalytic effect during photoreduction. On the other hand, for reduction by hydrazine, the I_D/I_G ratio increased to 1.20, indicating that the sizes of sp^2 domains of graphene were reduced by hydrazine treatment (24). The most remarkable feature in the Raman spectra of GO is the 2D band, and its position and shape can be used to distinguish the thickness of the films. As shown in Figure S2 in the Supporting Information, all the samples had broad 2D bands at about 2704 cm^{-1}, indicating that the present GO films exist as multinanosheet layers (50, 53).

Figure 3 shows some typical AFM images of the nanosheets. The GO nanosheets were about 1.2 nm thick prior to photoreduction, whereas they were about 0.8 and 0.7 nm thick after photoreduction in H_2 for 2 and 5 h, respectively. All of the obtained values in the thickness contained about 20% errors. The thicknesses measured between the GO nanosheets and the substrate are almost the same as those of the GO single nanosheets reported already (about 1.0 nm

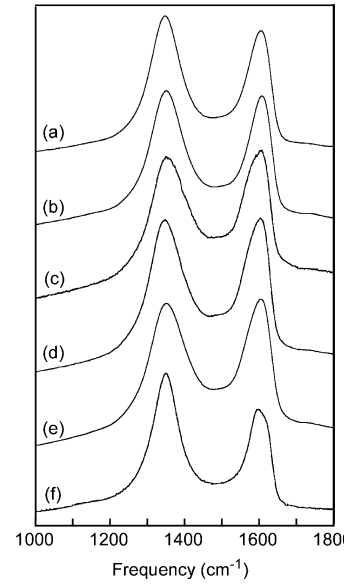

FIGURE 2. Raman spectra of aggregated nanosheet samples (sample 1): GO nanosheet (a) before photoreduction, (b) after photoreduction in H_2 for 2 h, (c) after photoreduction in H_2 for 5 h, and (d) after photoreduction in N_2 for 2 h. (e) Ag^+ adsorbed sample after photoreduction in H_2 for 2 h and (f) reduction by hydrazine.

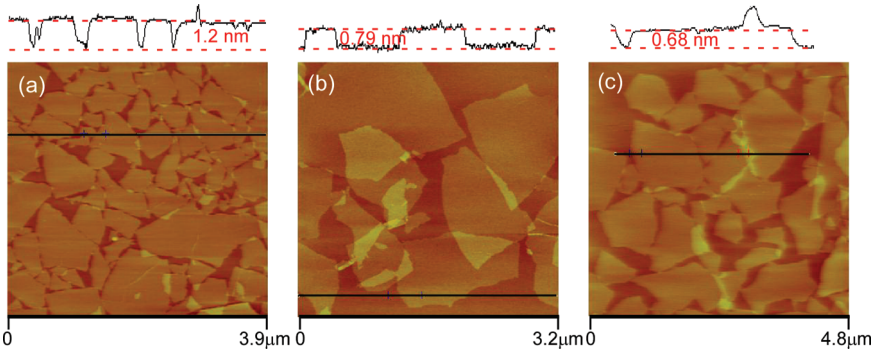

FIGURE 3. AFM images of single nanosheets (sample 3): (a) GO nanosheet, (b) after photoreduction in H_2 for 2 h, and (c) after photoreduction in H_2 for 5 h. Nanosheets *a*, *b*, and *c* are about 1.2, 0.8, and 0.7 nm thick, respectively.

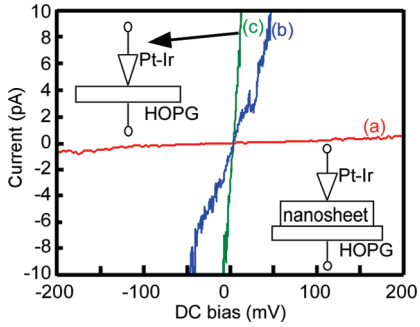

FIGURE 4. *I*−*V* curves of single nanosheets (sample 4): GO nanosheet (a) before and (b) after photoreduction in H_2 for 2 h and (c) HOPG. The conductivity increased dramatically after photoreduction in H_2.

18, 45). This implies that almost all the GO and reduced GO nanosheets in sample 3 are single. The thicknesses measured between the nanosheets (measured in the overlapping region between the nanosheets) were about 1.0, 0.7, and 0.6 nm for samples before photoreduction and after photoreduction in H_2 for 2 and 5 h, respectively; these thicknesses are smaller than those stated above. This observation is in agreement with that reported by Fernandez et al. (54). The GO nanosheet thickness increases with increasing degree of oxidation because oxygen-containing functional groups at the graphene surface increase the nanosheet thickness (18, 54). Consequently, the reduction in the nanosheet thickness by UV irradiation is due to photoreduction of the GO nanosheet.

Figure 4 shows *I*−*V* curves of the GO nanosheets (sample 4) measured by C-AFM. They represent the conductivity perpendicular to single GO nanosheets and the condition of the basal plane but not the edge of the GO nanosheet. The currents are small due to the very small contact area of the Pt−Ir AFM tip (10−10^2 nm). The nanosheet conductivity increased dramatically on UV irradiation in H_2 (which is similar to a semimetal). The *I*−*V* curve of the reduced GO nanosheet (sandwich sample consisting of HOPG/nanosheet/Pt−Ir AFM tip) was similar to that obtained when there was direct contact between HOPG and the Pt−Ir AFM tip. This implies that the conductivity of the reduced GO nanosheet is very high (especially at the basal plane but not at the edges). That is, the high conductivity is due to reduction of the epoxy group at the basal plane, as described above. On the other hand, the GO nanosheet was nearly insulating in the present applied voltage range. We were unable to distinguish between the conductivity of the sp^2 domain and that of the other oxygenated areas because these areas were much smaller (probably <10 nm^2) than the AFM tip.

Figure 5 shows *I*−*V* curves of nanosheet films prepared by (sample *a*) dipping a glass substrate with two Au electrodes into a nanosheet suspension and by (sample *b*) dropping the suspension onto the substrate. These *I*−*V* curves indicate the conductivities parallel to the GO nanosheets. Samples *a* and *b*, respectively, correspond to a single nanosheet and aggregated nanosheets (about 20 nm thick). AFM and SEM images of these samples are also shown in Figure 5. In sample *a*, some single nanosheets were deposited on the two Au electrodes. Consequently, the current in sample *a* was much smaller than that in sample *b* after photoreduction. Before photoreduction, the currents in both samples were less than about 0.1 pA at 1 V, whereas the currents were, respectively, about 50 nA and 20 μA for samples *a* and *b* after photoreduction (see Figure 5). The measured currents were almost the same for both samples photoreduced in H_2 and N_2. This indicates that the high conductivity is due to the destruction of C−O−C bonds in GO and the formation of relatively large sp^2 domains, but that it is not due to H addition (which may occur in H_2). The high conductivity of the reduced GO nanosheets is due to the increase in the sizes and numbers of sp^2 domains in the two-dimensional carbon network on reduction; electron hopping occurs between sp^2 domains (islands) in the sp^3 matrix formed by the oxygenated groups on the basal plane (40). The conductivities of the GO nanosheets reduced by the present technique were estimated to be higher than 10^3 Sm^{-1} if the conductivity of the GO increases by 10^5−10^6 times by the reduction from Figure 5, where the value of 0.0206 Sm^{-1} of GO powder (24) is used for the estimation. This value is almost in agreement with those of the GO nanosheets reduced by other techniques (18).

Photoreduction occurred even in the nanosheet suspension (sample 5). The suspension temperature did not change after photoreduction. The color of the suspension changed from light brown to black on photoreduction (see Figure 6a). Figure 6b shows UV−vis absorption spectra of the nanosheet suspensions. The black color and absorption in the visible region are due to the restoration of a sp^2 π-conjugated network (25) in the photoreduced GO nanosheets and their aggregation. AFM observations revealed that the nanosheets

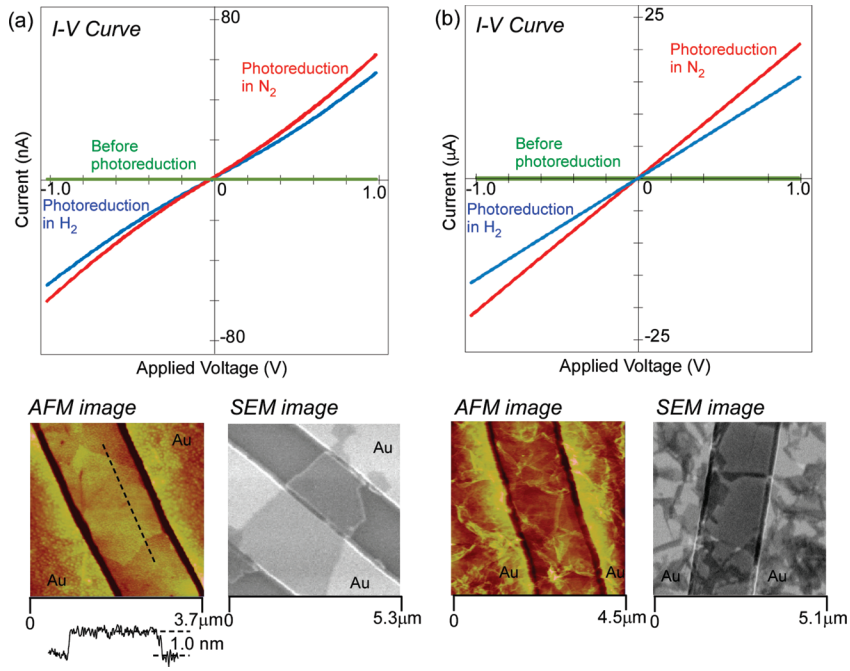

FIGURE 5. $I-V$ curves and AFM and SEM images of GO nanosheets on a comb electrode: (a) single GO nanosheet and (b) aggregated GO nanosheets. Photoreduction increased the conductivities by about 10^5-10^7 times. The AFM and SEM images in (a) confirm the presence of a single GO nanosheet on the electrodes.

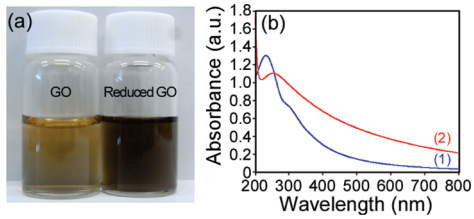

FIGURE 6. (a) Color depth and (b) UV−vis spectra of nanosheet suspensions (1) before and (2) after photoreduction in H_2 for 2 h (sample 5). Its color was black after photoreduction.

had various thicknesses ranging from 0.8 nm for a single nanosheet to 3 nm for aggregated nanosheets. Aggregation occurs due to the hydrophobic interaction between the photoreduced nanosheets in water; in contrast, a sufficiently oxidized graphene nanosheet is hydrophilic (22, 55). Figure S3 in the Supporting Information shows an XPS spectrum of the aggregated nanosheets after photoreduction for a sample prepared by dropping the suspension onto a Pt metal substrate. Photoreduction clearly reduces the intensities of the peaks at the binding energy of oxygenated groups. XPS analysis revealed that photoreduction in the suspension occurred for UV irradiation but not for visible light irradiation. These results reveal that photoreduction proceeds in the suspension only for UV irradiation.

Figure 7 shows photopatterning of sample 2. Figure 7a shows a schematic diagram of photopatterning using a carbon grid mesh as the photomask. Figure 7b shows SEM images of the photopatterned GO film. The white squares in the SEM images correspond to the irradiated GO surface that has a high conductivity. Thus, the present photoreduction process is very useful for photopatterning conductive areas of micrometer size on a GO nanosheet.

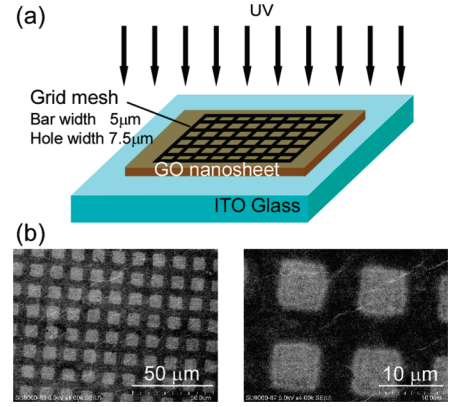

FIGURE 7. Photopatterning of GO nanosheets. (a) Schematic diagram of photopatterning and (b) SEM images of sample after photopatterning for 1 h in H_2.

CONCLUSIONS

Photoreduction of GO nanosheet without a photocatalyst proceeded easily under UV irradiation in H_2 or N_2, and it increased the conductivity of the nanosheet. In particular, UV irradiation when adsorbed Ag^+ was present resulted in very effective photoreduction. XPS and Raman spectroscopy analysis revealed that epoxy groups attached to the interior of aromatic domains in the GO nanosheet are mainly destroyed by UV irradiation and that they form relatively large sp^2 islands; this gives rise to the high conductivity. $I-V$ curves measured by C-AFM (perpendicular to a single nanosheet) and by a two-electrode system (parallel to a nanosheet) revealed that photoreduced GO nanosheets had high conductivities, whereas nonreduced GO was nearly insulating. Flash photopatterning of graphite oxide has been reported; it is quite different from our UV photoreduction process in principle because it is based on a photothermal effect (i.e., heat effect at temperatures higher than about 200

°C) obtained using a high power light source (56). This is similar to the case of laser photopatterning in the mechanism, as stated in Introduction section. Our photoreduction process will be more useful because the nanosheet temperature increases by very little (the surface temperatures of films during photoreduction were lower than about 40 °C) and micrometer size photopatterning is possible. Moreover, as stated above, the present process is useful even in suspension with no temperature change. When there are no impurities present (i.e., with no Ag^+), the present photoreduction technique is very useful as a simple photopatterning process that uses mild conditions. It will, thus, extend the applications of GO in many fields.

Supporting Information Available: A schematic of the comb electrode (Figure S1), Raman spectra of 2D bands (Figure S2), and XPS spectrum of the aggregated nanosheet (Figure S3). This material is available free of charge via the Internet at http://pubs.acs.org.

REFERENCES AND NOTES

(1) Geim, A. K.; Novoselov, K. S. *Nat. Mater.* **2007**, *6*, 183–191.
(2) Lee, C.; Wei, X.; Kysar, J. W.; Hone, J. *Science* **2008**, *321*, 385–388.
(3) Balandin, A. A.; Ghosh, S.; Bao, W.; Calizo, I.; Teweldebrhan, D.; Miao, F.; Lau, C. N. *Nano Lett.* **2008**, *8*, 902–907.
(4) Bolotin, K. I.; Sikes, K. J.; Jiang, Z.; Klima, M.; Fudenberg, G.; Hone, J.; Kim, P.; Stormer, H. L. *Solid State Commun.* **2008**, *146*, 351–355.
(5) Stoller, M. D.; Park, S.; Zhu, Y.; An, J.; Ruoff, R. S. *Nano Lett.* **2008**, *8*, 3498–3502.
(6) Zhang, Y.; Tan, Y. W.; Stormer, H. L.; Kim, P. *Nature* **2005**, *438*, 201–204.
(7) Akhavan, O.; Ghaderi, E. *J. Phys. Chem. C* **2009**, *113*, 20214–20220.
(8) Yang, K.; Zhang, S.; Zhang, G.; Sun, X.; Lee, S.-T.; Liu, Z. *Nano Lett.* **2010**, *10*, 3318–3323.
(9) Hu, W.; Peng, C.; Luo, W/; Lv, M.; Li, X.; Li, D.; Huang, Q.; Fan, C. *ACS Nano* **2010**, *4*, 4317–4323.
(10) Akahavan, O.; Ghaderi, E. *ACS Nano* **2010**, *4*, 5731–5736.
(11) Blake, P.; Hill, E. W.; Castro Neto, A. H.; Novoselov, K, S,; Jiang, D.; Booth, T. J.; Geim, A. K. *Appl. Phys. Lett.* **2007**, *91*, 063124.
(12) Rutter, G. M.; Crain, J. N.; Guisinger, N. P.; Li, T.; First, P. N.; Stroscio, J. A. *Science* **2007**, *317*, 219–222.
(13) Berger, C.; Song, Z.; Li, X.; Wu, X.; Brown, N.; Naud, C.; Mayou, D.; Li, T.; Hass, J.; Marchekov, A. N.; Conrad, E. H.; First, P. N.; de Heer, W. A. *Science* **2006**, *312*, 1191–1196.
(14) Ritter, K. A.; Lyding, J. W. *Nanotechnology* **2008**, *19*, 015704.
(15) Lotya, M.; Hernandez, Y.; King, P. J.; Smith, R. J.; Nicolosi, V.; Karlsson, L. S.; Blighe, F. M.; De, S.; Wang, Z.; McGovern, I. T.; Duesberg, G. S.; Coleman, J. N. *J. Am. Chem. Soc.* **2009**, *131*, 3611–3620.
(16) Dreyer, D R.; Park, S.; Bielawski, C. W.; Ruoff, R. S. *Chem. Soc. Rev.* **2010**, *39*, 228–240.
(17) Unal, U.; Matsumoto, Y.; Tanaka, N.; Kimura, Y.; Tamoto, N. *J. Phys. Chem. B* **2003**, *107*, 12680–12689.
(18) Park, S.; Ruoff, R. S. *Nat. Nanotechnol.* **2009**, *4*, 217–224.
(19) Eda, G.; Fanchini, G.; Chhowalla, M. *Nat. Nanotechnol.* **2008**, *3*, 270–274.
(20) Wang, X.; Zhi, L.; Müllen, K. *Nano Lett.* **2008**, *8*, 323–327.
(21) Robinson, J. T.; Perkins, F. K.; Snow, E. S.; Wei, Z.; Sheehan, P. E. *Nano Lett.* **2008**, *8*, 3137–3140.
(22) Becerril, H. A.; Mao, J.; Liu, Z.; Stoltenberg, R. M.; Bao, Z.; Chen, Y. *ACS Nano* **2008**, *2*, 463–470.
(23) Xu, Y.; Bai, H.; Lu, G.; Li, C.; Shi, G. *J. Am. Chem. Soc.* **2008**, *130*, 5856–5857.
(24) Stankovich, S.; Dikin, D. A.; Piner, R. D.; Kohlhaas, K. A.; Kleinhammes, A.; Jia, Y.; Wu, Y.; Nguyen, S. T.; Ruoff, R. S. *Carbon* **2007**, *45*, 1558–1565.
(25) Li, D.; Müller, M. B.; Gilje, S.; Kaner, R. B.; Wallace, G. G. *Nat. Nanotechnol.* **2008**, *3*, 101–105.
(26) Park, S.; An, J.; Piner, R. D.; Jung, I.; Yang, D.; Velamakanni, A.; Nguyen, S. T.; Ruoff, R. S. *Chem. Mater.* **2008**, *20*, 6592–6594.
(27) Geng, J.; Liu, L.; Yang, S. B.; Youn, S. C.; Kim, D. W.; Lee, J. S.; Choi, J. K.; Jung, H. T. *J. Phys. Chem. C* **2010**, *114*, 14433–14440.
(28) Chen, W.; Yan, L.; Bangal, P. R. *Carbon* **2010**, *48*, 1146–1152.
(29) Yang, D.; Velamakanni, A.; Bozoklu, G.; Park, S.; Stoller, M.; Piner, R. D.; Stankovich, S.; Jung, I.; Field, D. A.; Ventrice, C. A., Jr.; Ruoff, R. S. *Carbon* **2009**, *47*, 145–152.
(30) Akhavan, K. *Carbon* **2010**, *48*, 509–519.
(31) Zhang, Y.; Guo, L.; Wei, S.; He, Y.; Xia, H.; Chen, Q.; Sun, H.-B.; Xiao, F.-S. *Nano Today* **2010**, *5*, 15–20.
(32) Sokolov, D. A.; Shepperd, K. R.; Orlando, T. M. *J. Phys. Chem. Lett.* **2010**, *1*, 2633–2636.
(33) Zhou, Y.; Bao, Q.; Varghese, B.; Tang, L. A. L.; Tan, C. K.; S., C.-H.; Loh, K. P. *Adv. Mater.* **2010**, *22*, 67–71.
(34) Williams, G.; Seger, B.; Kamat, P. V. *ACS Nano* **2008**, *2*, 1487–1491.
(35) Kim, S. R.; Parvez, M. K.; Chhowalla, M. *Chem. Phys. Lett.* **2009**, *483*, 124–127.
(36) Williams, G.; Kamat, P. V. *Langmuir* **2009**, *25*, 13869–13873.
(37) Akhavan, O. *ACS Nano* **2010**, *4*, 4174–4180.
(38) Akhavan, O. *Carbon* **2011**, *49*, 11–19.
(39) Kaiser, A. B.; Gómez-Navarro, C.; Sundaram, R. S.; Burghard, S.; Kern, K. *Nano Lett.* **2009**, *9*, 1787–1792.
(40) Eda, G.; Lin, Y. Y.; Mattevi, C.; Yamaguchi, H.; Chen, H. A.; Chen, I. S.; Chen, C. W.; Chhowlla, M. *Adv. Mater.* **2010**, *22*, 505–509.
(41) Hummers, W. S., Jr.; Offeman, R. E. *J. Am. Chem. Soc.* **1958**, *80*, 1339.
(42) Shan, C.; Yang, H.; Song, J.; Han, D.; Ivaska, A.; Niu, L. *Anal. Chem.* **2009**, *81*, 2378–2382.
(43) An, S. J.; Zhu, Y.; Lee, S. H.; Stoller, M. D.; Emilsson, T.; Park, S.; Velamakanni, A.; An, J.; Ruoff, R. S. *J. Phys. Chem. Lett.* **2010**, *1*, 1259–1263.
(44) Cao, L.; Liu, Y.; Zhang, B.; Lu, L. *ACS Appl. Mater. Interfaces* **2010**, *2*, 2339–2346.
(45) Gao, X.; Jang, J.; Nagase, S. *J. Phys. Chem. C* **2010**, *114*, 832–842.
(46) Shen, J.; Shi, M.; Li, N.; Yan, B.; Ma, H.; Hu, Y.; Ye, M. *Nano Res.* **2010**, *3*, 339–349.
(47) Tuinstra, F.; Koenig, J. L. *J. Chem. Phys.* **1970**, *53*, 1126–1130.
(48) Ferrari, A. C.; Robertson, J. *Phys. Rev. B* **2000**, *61*, 14095–14107.
(49) Graf, D.; Molitor, F.; Ensslin, K.; Stampfer, C.; Jungen, A.; Hierold, C.; Wirtz, L. *Nano Lett.* **2007**, *7*, 238–242.
(50) Ferrari, A. C. *Solid State Commun.* **2007**, *143*, 47–57.
(51) Cançado, L. G.; Takai, K.; Enoki, T.; Endo, M.; Kim, Y. A.; Mizusaki, H.; Jorio, A.; Coelho, L. N.; Magalhães-Paniago, R.; Pimenta, M. A. *Appl. Phys. Lett.* **2006**, *88*, 163106.
(52) Akhavan, O.; Abdolahad, M.; Esfandiar, A.; Mohatashamifar, M. *J. Phys. Chem. C* **2010**, *114*, 12955–12959.
(53) Dato, A.; Radmilovic, V.; Lee, Z.; Phillips, J.; Frenklach, M. *Nono Lett.* **2008**, *8*, 2012–2016.
(54) Solís-Fernández, P.; Paredes, J. I.; Villar-Rodil, S.; Martínez-Alonso, A.; Tascón, J. M. D. *Carbon* **2010**, *48*, 2657–2660.
(55) Li, X.; Zhang, G.; Bai, X.; Sun, X.; Wang, X.; Wang, E.; Dai, H. *Nat. Nanotechnol.* **2008**, *3*, 538–542.
(56) Cote, L. J.; Cruz-Silva, R.; Huang, J. *J. Am. Chem. Soc.* **2009**, *131*, 11027–11032.

AM100900Q